Discrete Element Simulations of Dense Packings and Heaps made of Spherical and Non-Spherical Particles

H. G. Matuttis, S. Luding, and H. J. Herrmann
Institute for Computer Applications 1,
Pfaffenwaldring 27, D-70569 Stuttgart, GERMANY

June 16, 1999

Abstract

The Discrete Element Method (DEM) in the simulation of static packings allows one to investigate the behavior of granular materials by modeling the forces on the particle level. No macroscopic parameters like the angle of repose enter the simulation, but they can be extracted as a result of the particle properties like friction, roughness or shape. One of the issues of static packings recently discussed is the stress distribution under granular heaps. This problem is used to highlight the possibilities of modeling at the particle level using DEM. Phenomena like arching or stress-chains are observed even for spherical particles in a regular pile in the absence of friction if the bottom is rough. The situation does not change much if polygonal, frictional particles are used without disturbing the regular piling. For more realistic situations, when the pile is built by pouring grains from above, the packing and the stresses are influenced by the creation history. The more eccentric the polygons are, the more pronounced a dip is observed in the vertical stress under the apex of the sand-pile.

Keywords: DEM, numerical modeling, non-spherical particles, friction, sandpiles

1 Introduction

Many rather astonishing phenomena occur in flowing granular materials like sand or powders, as shown in numerous studies, review articles [1–7], books [8–13], and in this special issue of Powder Technology. The effects observed in granular media originate in the ability of the material to form a hybrid state between a fluid and a solid: When the density exceeds a certain value, i.e. the critical dilatancy threshold, it resists shear like a solid. When the overall density is sufficiently low, the granular medium can be regarded as fluid- or gas-like, situations which will not be considered in this study.

One of the many interesting features of granulates is the stress distribution in static or quasi-static arrays. In contrast to a liquid, the pressure in a silo filled with grains, does not increase linearly with depth, but saturates at a certain value [14]. This is due to internal friction and due to arching, so that the walls of the silo carry a part of the weight of the material. In sandpiles no walls are present so that the situation is different because the total weight of the pile has to be carried by the bottom. On a rather small scale, comparable to the size of a grain, stress chains are observed, i.e. stresses are mainly transported along selected paths, and the probability distribution of stress spans orders of magnitude [15–18]. The problem of stress propagation in granular packings has received much attention in the last years [17, 19–24] due to the pressure minimum which was observed experimentally in granular cones [25–29]. In granular wedges, however, no [30, 31] or only small [25] pressure minima could be observed. For a more detailed review of experimental and theoretical work see the paper by Savage in [13].

DEM Simulations of granular materials can also be applied to answer questions concerning the micro-mechanics [32–34] or to determine the constitutive behavior of granular soils [35–39]. Some effects in the mechanics of granular materials cannot be modeled by using particles of simple spherical geometries. Simulations of ellipses [40] gave already first promising results concerning the behavior of the maximal shear-stress [41, 42]. Apart from ellipses, super-quadrics [43], continuously connected circular segments [44], and polygons [45–49] have been used for a more flexible modeling of the particle geometries and the boundaries. The aim of this paper is to give an insight into the Discrete Element Modeling of spherical and polygonal particles. The physical system (or boundary condition) chosen as an example is the sandpile. First, the "microscopic" point of view is introduced – particles interact via contact forces. The alternative way of describing a granular material is treating it as a macroscopic continuum, where stress has to be defined. One goal of this paper is to present a way to obtain such "macroscopic" informations from DEM [36, 50, 51].

Section 2 is dedicated to the microscopic viewpoint, i.e. the introduction of the modeling approaches for spheres and polygons. In particular we will present force laws used for the "soft-particle" Molecular Dynamics (MD) [52, 53], adjusted for inelastic particles with frictional forces [54–56]. In section 3, averaging procedures are introduced to obtain macroscopic quantities from a micro-description and, in section 4, quasi-static granular assemblies are modeled using smooth, spherical particles [23]. Finally, in section 5, the influence of the particle eccentricity and of the building history are examined for frictional, polygonal particles [24]. The results and consequences of the presented data are summarized and discussed in section 6.

2 Modeling soft particles

The elementary units of granular materials are mesoscopic grains consisting of many atoms each ($10^{15} - 10^{25}$). In order to account for the excluded volume, one usually assumes that

the grains are impenetrable but deform under stress. (Other models which assume perfect rigidity are not discussed here.) In order to model realistic granular materials with DEM, the aims to treat large particle numbers and to model the particle contacts in full detail have to be weighed against each other. Since the realistic modeling of the deformations of spherical particles in the framework of a continuum theory [57, 58] would be much too complicated, we relate the interaction force to the overlap of two particles. The results of such a model have to be validated by comparison with experimental measurements [59–61]. The overlap δ is used to define a potential like in conventional molecular dynamics simulations, leading to forces that are material dependent and involve properties such as Young's modulus of elasticity. Finally, we neglect attractive forces and the presence of other phases and thus focus on "dry granular media".

When all forces acting on a particle i, either from other particles or from boundaries, are known, the problem is reduced to the integration of Newton's equations of motion for the translational and the rotational degrees of freedom

$$m_i \frac{\mathrm{d}^2}{\mathrm{d}t^2}\vec{r}_i = \vec{f}_i \ , \quad \text{and} \quad I_i \frac{\mathrm{d}^2}{\mathrm{d}t^2}\vec{\Phi}_i = \vec{M}_i \tag{1}$$

The mass of particle i is denoted as m_i, and its moment of inertia is $I_i = q_i m_i (d_i/2)^2$ with the dimensionless shape factor q_i. The vectors $\vec{r}_i$ and $\vec{\Phi}_i$ give the position and the orientation in space of particle i, respectively. Interactions are short range and active on contact only, so that the total force (torque) on particle i is $\vec{f}_i = \sum_c \vec{f}_i^{\,c}$ ($\vec{M}_i = \sum_c \vec{M}_i^c$), where the sum runs over all contacts c of particle i. The torque $\vec{M}_i^c = \vec{l}_i^{\,c} \times \vec{f}_i^{\,c}$ is related to the force $\vec{f}_i^{\,c}$ via the branch vector $\vec{l}_i^{\,c}$ from the particle center to the point of contact c. Eq. (1) consists of six scalar equations in three dimensions and reduces to three in two dimensions (2D). Frequently used force laws accounting for excluded volume, dissipation, and friction will be introduced in the following.

2.1 Spherical particles

The interaction range for grains is short, i.e. the particles interact only when they are in contact so that their overlap $\delta = \frac{1}{2}(d_1 + d_2) - (\vec{r}_1 - \vec{r}_2) \cdot \vec{n}$ is positive. The diameter and the position of the center of mass are denoted as d_i and $\vec{r}_i$ $(i = 1, 2)$, respectively, and the unit vector that connects the particles' centers of mass, pointing from 2 to 1, is $\vec{n} = (\vec{r}_1 - \vec{r}_2)/|\vec{r}_1 - \vec{r}_2|$.

The first contribution to the force acting on particle 1 from 2 – accounting for the excluded volume which each particle occupies – is an elastic repulsive force

$$\vec{f}_{\mathrm{el}} = k_n \delta_0 (\delta/\delta_0)^\nu \vec{n} \ , \tag{2}$$

where k_n/δ_0 is Young's modulus of elasticity and δ_0 is a normalization constant, an effective particle diameter depending on the non-linearity ν and the particle shape. In the simplest case of a linear spring that follows Hooke's law, one has $\nu = 1$ and can regard k_n as the spring constant with unit [N/m]. In the case of elastic spheres, the Hertz contact law is obtained with $\nu = 3/2$ [62, 63], whereas for conical contacts $\nu = 2$ could be used. Plastic and thus hysteretic interaction laws [64, 65], which are relevant for large stresses and large impact velocities are not discussed here, since we are interested in quasi-static-situations.

The second contribution, a viscous dissipation, is given by the damping force in the normal direction

$$\vec{f}_{\mathrm{diss}} = \gamma_n \dot{\delta} (\delta/\delta_0)^\psi \vec{n} \ , \tag{3}$$

where γ_n is a phenomenological viscous dissipation coefficient with units [kg s^{-1}] and $\dot{\delta} = -\vec{v}_{12} \cdot \vec{n} = -(\vec{v}_1 - \vec{v}_2) \cdot \vec{n}$ is the relative velocity in the normal direction. The exponent ψ accounts for the non-linear dissipation-overlap relation.

The simple linear spring-dashpot model with $\nu = 1$ and $\psi = 0$ can be solved analytically and leads to a contact duration $t_c = \pi/\omega$ and a coefficient of restitution $r = \exp(-\eta t_c)$, with $\omega = \sqrt{\omega_0^2 - \eta^2}$, $\omega_0^2 = k_n/m_{12}$, $\eta = \gamma_n/(2m_{12})$, and $m_{12} = m_1 m_2/(m_1 + m_2)$ [56]. Consequently, the ratio η/ω_0 determines whether one can regard the collision as the half of a damped oscillation for $\eta/\omega_0 < 1$ or as an overdamped situation for $\eta/\omega_0 > 1$. As a cautionary note, we remark that it is *not* appropriate to identify the end of the contact (of non-cohesive particles) strictly with $t = t_c$, since in *dynamical* collisions, the form of Eq. (3) leads to discontinuities in the total force $\vec{f}_n = \vec{f}_{\rm el} + \vec{f}_{\rm diss}$ at the beginning ($t = t_0$) and the ending ($t = t_0 + t_c$) of the overlap (where $f_n(t_c)$ is also attractive [56]). This non-smoothness of the contact force vanishes when $\psi > 0$ is used in Eq. (3), where $\nu = 3/2$ and $\psi = 1/2$ are a reasonable choice for the modeling of viscoelastic spheres [66–68].

The third contribution to the contact force – accounting for tangential friction – can be chosen in the simplest case as $\vec{f}_{\rm shear} = -\gamma_t \dot{\xi} \vec{t}$, where γ_t is the viscous damping coefficient in tangential direction and $\dot{\xi} = \vec{v}_{12} \cdot \vec{t}$ is the tangential component of the relative velocity, with $\vec{t} = \vec{v}_{12}/|\vec{v}_{12}|$. (This $\vec{t}$ is somewhat different from the frequently used tangential unit-vector that one gets by simply rotating $\vec{n}$ about 90 degrees.) For many applications (arching, heap formation) it is, however, important to incorporate models which more closely approximate static friction [32, 55, 64, 65, 69, 70]: When two particles get into contact at time t_0, one assumes a "virtual" spring between their contact points, where

$$\xi = \left(\int_{t_0}^{t} \vec{v}_{12}(t') dt' \right) \cdot \vec{t} \tag{4}$$

is the *total* tangential displacement of this spring at time t, built up during the contact duration $t - t_0$. Note that in our definition of the tangential velocity, the tangential unit vector points in the direction of the tangential relative velocity so that $\vec{v}_{12} \cdot \vec{t}$ would be always positive, if the scalar product would be inside the integral. In Eq. (4), ξ can be either positive or negative so that $\vec{\xi} = \xi \vec{t}$ can also be anti-parallel to $\vec{t}$. The restoring (static) frictional force, $\vec{f}_{\rm static} = -k_t \vec{\xi}$, with the stiffness of the tangential spring k_t, can thus be oriented parallel *or* anti-parallel to $\vec{t}$. This fact is a necessary ingredient to obtain a positive tangential restitution as Foerster et al. [59] find from experiments on various materials.

According to Coulomb's criterion $f_t \leq \mu f_n$, the tangential force is smaller than (or equal to) the normal force f_n at the contact, with the friction coefficient μ. Cast into a formula this gives the friction force

$$\vec{f}_t = -\frac{\vec{\xi}}{|\vec{\xi}|} \min(k_t |\vec{\xi}|, \mu f_n) \ . \tag{5}$$

We note that the tangential force at a contact (and thus the maximum elongation of the tangential spring $\xi_{\rm max}$) has to be limited by the relation $k_t \xi_{\rm max} = \mu f_n$ in order to account for sliding and to lead to reasonable agreement with contact dynamics simulations or theoretical calculations [70, 71].

The formulation of the interaction laws for spherical particles in this subsection can be used in two and three dimensions, even when the detailed calculations of the deformation geometry become much more complicated. In contrast, the following formulation for polygons is limited to two dimensions.

2.2 Polygonal Particles

The simplest way to model non-spherical particles is to connect several spherical particles by springs to form a square or a triangle [72, 73]. However, we prefer to introduce convex polygonal particles in 2D and then define the interaction laws used later for the simulations of sandpiles (for alternative approaches see [43, 46, 74–76]). The polygons used in the following are convex with C edges and are inscribed into an ellipse with axis a and b of different length. The number of edges defines the smoothness of the polygon and the eccentricity a/b of the ellipse its deviation from a circular shape. In the case of round particles, the direction of the active forces is well defined but, for polygonal particles, one has to choose an appropriate direction for the interaction force between particles. Due to the particle shape, the contact force will, in general, *not* point to the center of mass of a particle, so that torques are present in the absence of tangential forces. The forces defined below, and the algorithm introduced for polygonal particles, can be directly adapted for other non-spherical geometries like ellipses or superquadrics [43, 44].

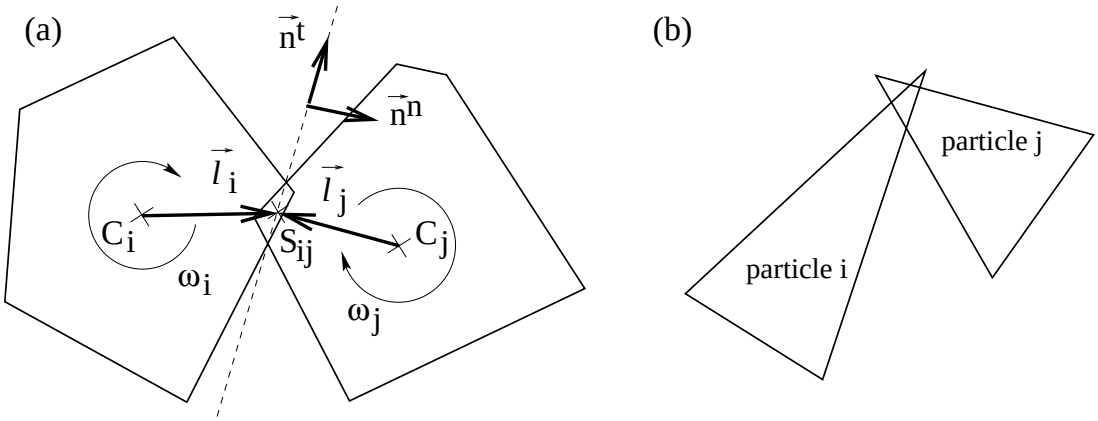

Figure 1: (a) Schematic drawing of a particle-particle contact for two polygons. (b) Sketch of an ambiguous contact direction for the collision of sharp corners.

We characterize the orientation of the overlap area (with surface A) of two polygons, see Fig. 1(a), by the intersection line (dashed line) that connects the two crossing points of the two polygon outlines (solid lines). Relative to this line the force is decomposed into its normal and its tangential direction, both characterized by the unit vectors $\vec{n}^{\rm n}$ and $\vec{n}^{\rm t}$, respectively. These directions are unique as long as there is no intersection between two "spikes" (triangles with very small angle), as shown in Fig. 1(b). Algorithms which treat ambiguities of this type have been given in Refs. [77–80].

The *force point* S_{ij}, see Fig. 1(a), is defined as the center of the intersection line of the two overlapping polygons i and j; however, the center of the overlap polygon could be used as well. The vector from a particle's center of mass $\vec{r}_i$ to the force point is denoted as $\vec{l}_i$. The forces which the two particles in contact exert on each other act at the force point with opposite direction, respectively.

2.2.1 The Normal Force

As in the case of spheres, the normal force consists of two components $f^{\rm n} = f^{\rm n}_{\rm el} + f^{\rm n}_{\rm diss}$, a repulsive part $f^{\rm n}_{\rm el}$, and a dissipative part $f^{\rm n}_{\rm diss}$. (Here the superscript $^{\rm n}$ indicates that polygons are used.) The formulation of the force laws is different from that in the previous subsection, since the particle shape has to be taken into account. Two overlapping particles are assumed

to deform in such a way, that the overlap area is a measure of the deformation and is thus proportional to the force between the two particles, in analogy to the argument used in subsection 2.1 for spherical particles. We use the force law

$$f_{\rm el}^{\rm n} = k^{\rm n}(A/l) \ , \tag{6}$$

with the distance between the centers of mass and the force points $l_i = |\vec{l}_i|$ giving the typical length $l = 1/(1/l_i + 1/l_j)$ for two particles i and j at their common contact point. This choice is arbitrary; it is based on the assumption that a stack of solid bricks should behave similar to a large brick of the same height. Note that $k^{\rm n}$ corresponds to k_n with units [N/m], and A/l corresponds to the length $\delta_0(\delta/\delta_0)^\nu$ in Eq. (2). In general, the choice of the contact force proportional to the overlap area leads to a dependence of the collision time on the contact geometries. The damping force

$$f_{\rm diss}^{\rm n} = \gamma^{\rm n}\frac{{\rm d}(A/l)}{{\rm d}t} \ , \tag{7}$$

is modeled like the dissipative force in Eq. (3), with the dimensionless damping constant $\eta^{\rm n} = \gamma^{\rm n}/\sqrt{m_{12}k^{\rm n}}$, a measure for the strength of dissipation. If $\eta^{\rm n} \ll 1$, the dissipation is rather weak and if $\eta^{\rm n} > 1$ the oscillator made up by $f_{\rm el}^{\rm n}$ and $f_{\rm diss}^{\rm n}$ and the two masses is overdamped.

2.2.2 The Tangential Force

The tangential force $\vec{f}^{\rm t}$ is modeled as a harmonic oscillator, similar to Eq. (5). The elongation of the tangential spring is incremented proportional to the relative tangential velocity, see Eq. (4), and $\vec{f}^{\rm t}$ is proportional to the tangential stiffness $k^{\rm t} = \frac{2}{7}k^{\rm n}$. The value of 2/7 causes the normal and the tangential springs to react in similar time scales, so that the eigen-frequencies of the normal and tangential oscillator are comparable, at least in the case of spheres [56]. It is also necessary to include a damping in the tangential direction, in order to avoid undesired long-lasting tangential oscillations. A tangential viscous term $-\gamma^{\rm t}\dot{\xi}$ is added to the elastic tangential repulsive force and the sum is truncated if it is larger in magnitude than $\mu f^{\rm n}$, according to Coulomb's law, similar to Eq. (5). For the dimensionless tangential dissipation we use $\eta^{\rm t} = \gamma^{\rm t}/\sqrt{m_{12}k^{\rm t}} = 0.01$ throughout this paper. A more extensive discussion on the implementation of tangential forces can be found in [55, 70]. Alternative formulations for force laws of polygonal particles have been given in [46, 48, 79, 81].

3 From the micro- to a macro-description

In the previous section, the microscopic point of view was introduced, as used in the discrete element method. Particles are viewed as independent entities which interact when they come in contact. In this framework, the knowledge of the forces at each contact is sufficient to model the dynamics and the statics of the system. Tensorial quantities like the stress or the deformation gradient are not necessary for a discrete modeling, but the subject of current research is to establish a correspondence to continuum theories by computing from DEM tensorial quantities such as the stress σ [33, 51, 82]. In the static case the stress tensor is usually defined as the dyadic product of the force $\vec{f}^c$ and the branch vector $\vec{l}^c$ (from the particle center to contact point c), so that its components are

$$\sigma_{\alpha\beta} = (1/V)\sum_c \ f_\alpha^c l_\beta^c \ , \tag{8}$$

where the indices α and β indicate the cartesian coordinates, i.e. the horizontal x and the vertical z in 2D. This stress tensor is an average over all contacts of the particles within the

volume V. In order to carry out the averaging in Eq. (8) one can sum over the contacts of only one particle [23]. In this case V has to be chosen so that all average volumes cover the whole system, a rather difficult task in the case of moving, polydisperse, possibly polygonal particles. The one-particle averaging will thus be applied in the situation of almost monodisperse spherical particles only. The alternative is to put a grid with cell-size V over the system and to use all contacts, related to particles with their center of mass in the respective cell, for the sum in Eq. (8). In order to suppress the fluctuations, we either average over many realizations, or we use the so-called "moving averages". In the latter case, the cells of the grid are about ten particle diameters large and can overlap each other in horizontal direction.

From a static configuration of "soft" particles one may now calculate the components of the stress tensor $\sigma_{xx}, \sigma_{zz}, \sigma_{xz}$, and σ_{zx} and also define $\sigma^+ = (\sigma_{xx} + \sigma_{zz})/2$, $\sigma^- = (\sigma_{xx} - \sigma_{zz})/2$, and $\sigma^* = (\sigma_{xz} + \sigma_{zx})/2$. If tangential forces are neglected, the particles are torque-free and we observe only symmetric stress tensors, i.e. $\sigma_{zx} = \sigma_{xz}$ [23]. The eigenvalues of σ are thus $\sigma_{max,min} = \sigma^+ \pm \sqrt{(\sigma^-)^2 + (\sigma^*)^2}$, and the major eigenvalue is inclined at an angle

$$\phi = \arctan\left(\frac{\sigma_{max} - \sigma_{xx}}{\sigma_{xz}}\right) = \frac{\pi}{2} + \frac{1}{2}\arctan\left(\frac{2\sigma_{xz}}{\sigma_{xx} - \sigma_{zz}}\right) \tag{9}$$

to the horizontal in the counterclockwise direction.

Since we are interested in 2D sand-piles, the horizontal coordinate x can be scaled by the width l of the pile, i.e. $X = x/l$, so that $X = 0$ and $X = 1$ correspond to the lower left and right ends of the pile, respectively. In order to find a reasonable scaling for the stresses, we assume [20, 83], as a simplified example, a rigid triangle with the density ρ, the width l, the height h, and the mass $m = \rho h l/2$. Due to the rigidity, we find a constant force at the supporting flat surface, so that the pressure is also constant $p = mg/l = \rho g h/2$. Thus we will scale the stress by the pressure p and then use the dimensionless stress tensor $S = 2\sigma/(\rho g h) = \sigma l/(mg)$. Apart from the components of S we will plot the stress tensor in its principal axis representation in the next sections, i.e. for each particle the scaled major principal axis is oriented along ϕ while the minor axis is oriented perpendicular to it, where the length of the axis is proportional to the magnitude of the eigenvalues.

In contrast to dynamic situations, the central problem in static simulations is to reach a force equilibrium, when the particles come to a halt. A totally static situation is not easily achieved with DEM, however, one has the criterion that the kinetic energy has to be orders of magnitude smaller than the elastic energy stored in the contacts. The DEM method is not necessarily the best choice to achieve statics, for a faster relaxation, implicit schemes can be more efficient [36, 84]. Since we are interested in static arrangements of particles in the gravitational field, we use rather strong dissipation, in order to reach the steady state as quickly as possible. However, even when the DEM method is not the best choice for a fast relaxation, the closing and opening of contacts is implemented straightforwardly. First, smooth, spherical particles with different force laws are used to explore how far such a simplified model can explain, for example, the pressure dip. Then, polygonal, frictional particles are used to better approximate real systems.

4 Results for spherical particles

In the simulations presented in this section, N spherical particles with diameters d_i (i = 1,...,N) are used. If not explicitly mentioned, monodisperse spheres of diameter $d_i = d_0$ = 1.5 mm are employed. The N particles are placed into a container with different boundary conditions at the bottom and also different system sizes. Starting from a regular, closely

packed triangular arrangement with L particles in the lowermost layer $M = 0$ at the bottom, heaps of slope 60^o or 30^o can be modeled by forming layer M with $L_M = L - M$ or $L_M = L - 3M$ particles, respectively, as displayed in Fig. 2. The number of particles is thus $N^{(60)} = H^{(60)}(L+1)/2$ or $N^{(30)} = H^{(30)}(L - 3(H^{(30)} - 1)/2)$ with the number of layers $H^{(60)} = L$ or $H^{(30)} = \text{int}[(L-1)/3] + 1$. The largest simulated pile has $L = 100$ and thus $N^{(30)} = 1717$ particles.

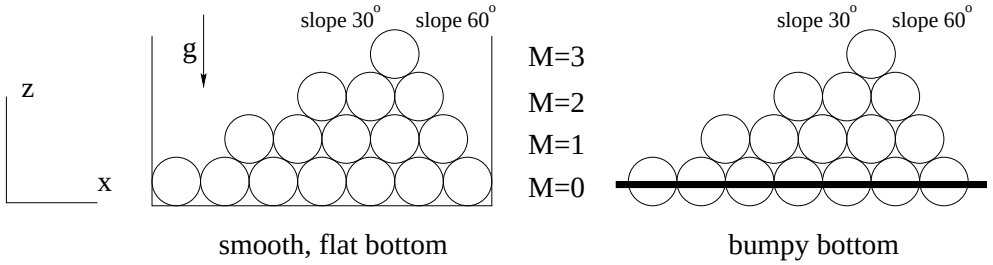

Figure 2: Schematic drawing of a pile in a box with smooth, flat bottom (left), and on a bumpy bottom (right), with $L_0 = 7$. The solid bar at the right indicates that the particles in row $M = 0$ are fixed, so that the first relevant row with mobile particles is $M = 1$ with here $L_1 = 5$.

The initial velocities and overlaps of the particles are zero, gravity is slowly increased from zero to the selected magnitude and the system is simulated until the kinetic energy is several orders of magnitude smaller than the potential energy, and the stresses no longer vary with time. The particles at the bottom layer $M = 0$ are either fixed, or may slide horizontally and penetrate the bottom vertically. When sliding is allowed only the outermost particles are horizontally fixed by the sidewalls.

Here, we focus on properties of granular systems in the absence of friction. By neglecting solid friction, we will examine to what extent phenomena like stress chains and arching depend on friction. However, we are confronted here with what could be called "geometrical friction" or "arching", as the particles restrict the motion of their neighbors due to excluded volume effects; this makes it possible to create a stable pile [23, 85]. The parameters are chosen so that the maximum overlap is much smaller than the particle radius. Besides this requirement, the data presented in the following are scaled so that different sets of parameters lead to similar pictures.

4.1 A Small Variation of the Width of the System

Here, a 30^o pile, with $L_1 = 19$, on a bumpy bottom, see Fig. 2, is simulated, and the separation $d_0(1+c)$ of the fixed particles in the lowermost row $M = 0$ is varied. The values of c are $c = 1/15$, 0, -1/750, and -1/150. In Fig. 3(a) and (c) the vertical and horizontal components of the stress tensor are plotted and, in Fig. 3(b) and (d), the contact network and the principal axis of the stress tensor are displayed respectively. The interesting result is that the vertical stress in Fig. 3(a) has a dip for negative c, the depth of which increases with increasing magnitude of c [20, 23]. The horizontal stress in Fig. 3(c) is much larger for negative c than for positive c.

From Fig. 3(b) one finds a translation invariant diamond lattice for the contacts only for $c = 1/15$, i.e. a wide spacing between the particles. In this case, the vertical stress $S_{zz}(1)$ has a zig-zag structure that is related to the steps at the surface of the 30^o pile. For a spacing with $c = 0$ and $c = -1/750$ we have a contact network with regions of coordination number 4 and 6, corresponding to the diamond or the triangular contact network. For strongly

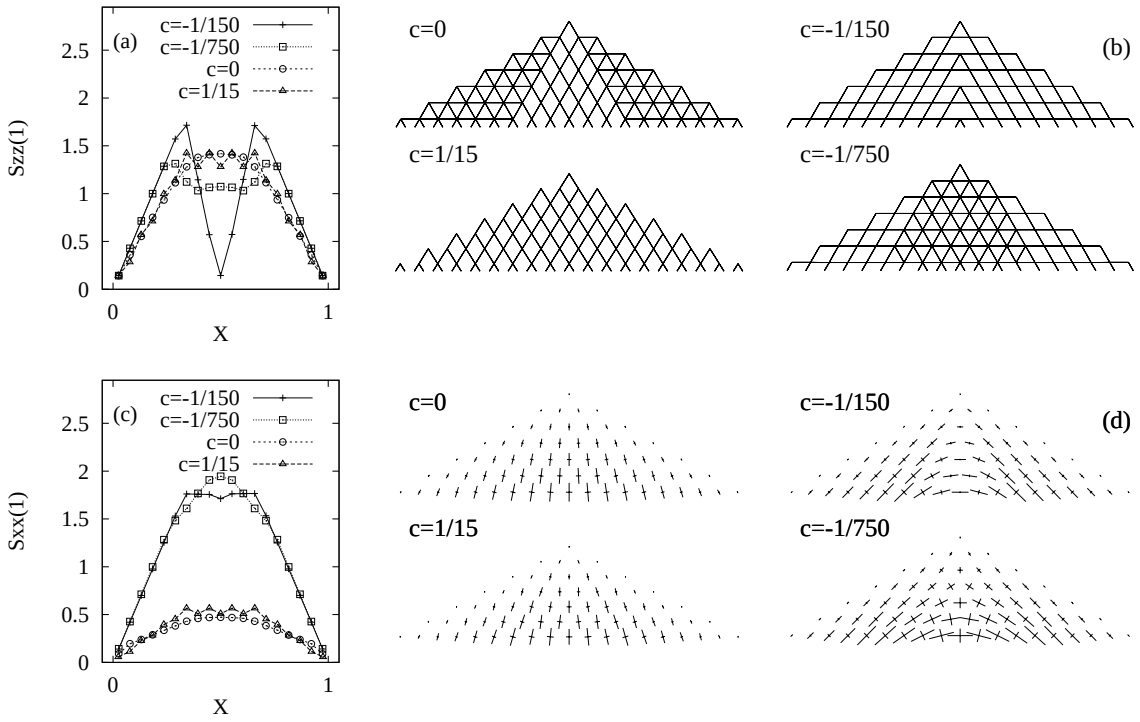

Figure 3: (a) Dimensionless vertical stress $S_{zz}(1)$, in row $M = 1$, vs. dimensionless horizontal coordinate $X = x/l$ for a 30^o pile with bumpy bottom and $L_1 = 19$. The particles in row $M = 0$ are fixed at a distance $d_0(1 + c)$, i.e. they are squeezed together for negative c or separated for positive c. (b) The contact networks for the corresponding systems. (c) Horizontal stress $S_{xx}(1)$, vs. X. (d) The principal axis of the stress tensor for the corresponding systems, from [23].

squeezed bottom particles, i.e. $c = -1/150$, the contact network is again a diamond lattice, but the longer axis of the diamond is tilted away from the vertical. From Fig. 3(d) we obtain arching for negative c and no arching for positive c. Evidently, a tilted diamond lattice is correlated to an arch in this situation. If also the angle ϕ is calculated, we observe a fixed value only for $c < 0$, in the outer part – consistent with the fixed principal axis (FPA) theory by Wittmer et al. [22, 86].

From a detailed comparison of the contact network to the stress tensor we may conjecture two facts. First, the ratio of the principal axis $s = S_{\min}/S_{\max}$ seems to determine whether the contact network is of triangular or diamond structure [87]. For $c = 0$ and for $c = -1/750$ the triangular contact network is formed if s is large (the larger s, the more isotropic is the stress). Second, the orientation of the diamonds is correlated to the orientation of the stress tensor, i.e. the longer axis of the diamond lattice (for negative c) is more or less parallel to the direction of the eigenvector related to the major eigenvalue.

One main result is that arching and the dip in the vertical stress at the bottom are not necessarily due to solid friction [20, 87, 88]. When the contact network is tilted away from the vertical, stresses are preferentially propagated outwards; this may be regarded as a reason for arching and for the dip, but only due to the anisotropy of the contact network, and neither due to friction nor due to non-spherical particle shapes. The contact network varies within the pile, i.e. if the material properties are inhomogeneous, stresses different from theoretical predictions based on the assumption of a regular network are observed.

4.2 An exact solution

Instead of a numerical integration of Newton's equations of motion, one can also use a symbolic calculation software to get *exact* results after assuming a static situation with all velocities vanishing [85, 89]. The interaction used is equivalent to Eq. (2) with $\nu = 1$. Here, different from Eq. (2), the discs are supposed to be stiff, i.e. $k_n \gg m/d_0$, so that the overlap δ of discs is always infinitesimal, and the limit $k_n \to \infty$ is implied for the solution.

For the comparison of the DEM results with the exact solution we use a pile of base width $L_0 = 16$, a slope of 30^o, and put it on a smooth surface fixing only the corner-stones. Comparing the exact solution with the numerical simulations, we obtain a very good agreement in Fig. 4. The principal axis representation (left, the scaling is different at top and bottom) and the contact network (right), with the line-width proportional to the force, show almost perfect agreement, except for one detail. Since the particles used for the numerical simulation are less stiff than those used for the analytical solution, two more contacts at the bottom, symmetric and next to the center, are open. Varying the width of the system the numerical simulations from the previous subsection are confirmed. An accentuation of the dip is obtained when applying a compressive force on the corner stones. A discussion of these results can be found in [85].

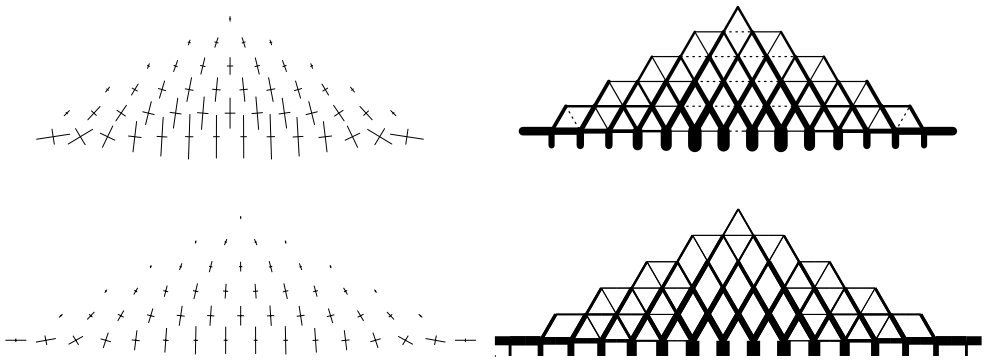

Figure 4: Comparison of the exact results (top) to the numerical simulation (bottom) for a heap with 30^o slope, $L_0 = 16$, on a smooth, flat bottom. The two outermost particles are skipped for the exact calculations.

4.3 Nonlinear force-laws

The situation addressed here is a homogeneous 30^o pile, in which $L_0 = 100$ particles in row $M = 0$ are used. The particles in the lowermost row are fixed with $c = 0$ so that the horizontal separation is d_0. We compare the contact networks for linear ($\nu = 1$) and nonlinear ($\nu = 3/2$) normal interactions of Eq. (2) in the left and right half of the symmetric piles in Fig. 5 respectively. We observe a region with a diamond-lattice in the center of the pile and a triangular contact network at the shoulders, as in Fig. 3 for $c = 0$. Only in a thin layer close to the surface we find a diamond-lattice tilted outwards from the center. The contact network, is the same for both interaction laws, except for some weak deviations along the line where the two different networks meet each other and along the surface of the pile.

In Fig. 6(a) we plot the components of the dimensionless stress tensor $S(1)$ against X for the lowermost row of mobile particles, $M = 1$. Ignoring small deviations (the curves are more rounded for the linear interaction law), the stress tensor is the same in all cases $\nu = 1$, $\nu = 3/2$, and $\nu = 2$. Note that the data for $\nu = 2$ are obtained from simulations

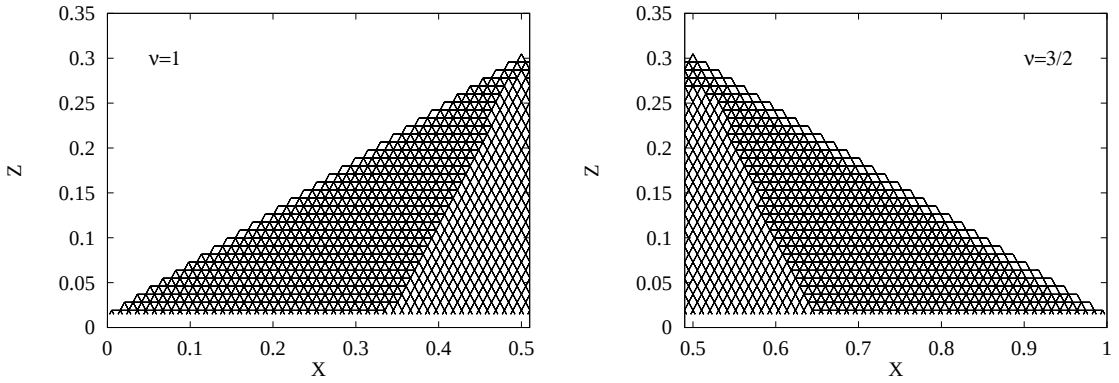

Figure 5: Half views of the contact network for simulations with linear (left) and nonlinear (right) interaction laws.

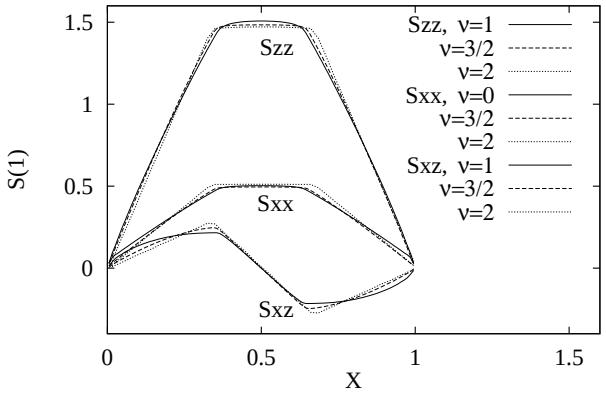

Figure 6: Components of the dimensionless stress tensor $S(1)$ at row $M = 1$ vs. dimensionless horizontal coordinate $X = x/l$, for a pile with immobile particles at the bottom, $M = 0$. The slope of the pile is 30^o and $L_0 = 100$. We use linear $\nu = 1$, and nonlinear interactions $\nu = 3/2$, see the inset. The data with $\nu = 2$ correspond to simulations with polygonal particles, as discussed in more detail in subsection 5.2.

of polygons with $C = 12$ sides, as described in the following section. If the stress ratio S_{xx}/S_{zz} is plotted, one observes a value of $1/3$ inside the pile, independent of ν. The value of $1/3$ is consistent with the predictions in Ref. [22] for a diamond contact network and can also be understood from geometrical arguments. Since the horizontal contact is open, the stiffness of the material is smaller in the horizontal direction than in the vertical direction. In the horizontal direction, there is a contribution of $k_n \cos 60^o$ to the stiffness over a vertical distance $d_0 \sin 60^o$. On the other hand, in the vertical direction there is a contribution of $k_n \cos 30^o$ to the stiffness over a horizontal distance $d_0 \sin 30^o$. Assuming a homogeneous deformation we arrive at $S_{xx}/S_{zz} = \tan^2 30^o = 1/3$.

From the stress tensor S in Cartesian coordinates we move to the principal axis system, where S is defined by the minor and major eigenvalues $S_{\min}$ and $S_{\max}$ and the angle of orientation ϕ as defined in Eq. (9). We plot the ratio of the eigenvalues $S_{\min}/S_{\max}$ in Fig. 7(a), the angle $\phi(1)$ in Fig. 7(b), and the minor and major eigenvalues in Fig. 7(c). Except for boundary effects close to $X = 0$ and $X = 1$ we have three regions which may be identified with the contact network regions in Fig. 5. In the center the stresses are almost constant and decrease in the outer part of the pile until they vanish at the boundary. Except for the

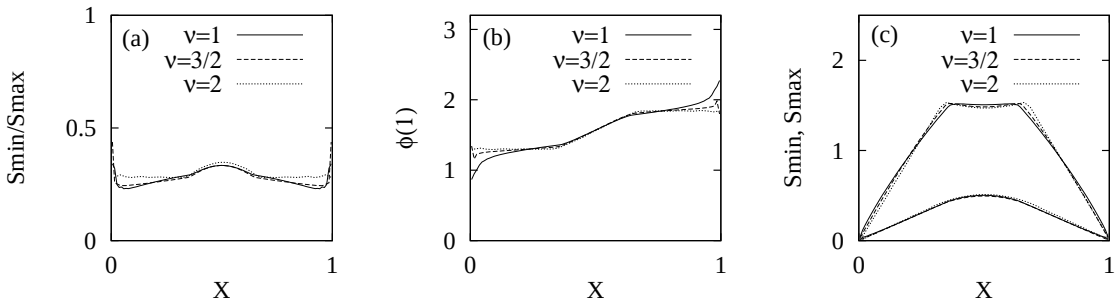

Figure 7: (a) Ratio of the eigenvalues of the stress tensor at row $M = 1$ vs. X, for the piles from Fig. 6. (b) The angle ϕ about which the major principal axis is tilted from the horizontal in counterclockwise direction. (c) The minor and major eigenvalues $S_{\min}$ and $S_{\max}$.

center, the stress tensor is always oriented outwards from the center. The orientation angle ϕ is almost constant in the outer regions and a transition takes place in the inner region.

In summary, we do not find essential qualitative differences when using frictionless particles with linear or non-linear force laws, and even for frictionless polygonal particles, not much difference is obtained.

4.4 Polydisperse Particles

Starting from a monodisperse 30^o pile with a bumpy bottom and $L_0 = 100$, we change the particle size of each particle slightly to the diameter $d_i = d_0(1 + r_d^i)$, where r_d^i is a random number homogeneously distributed in the interval $[-r_d/2, r_d/2]$. The vertical stress at the bottom is plotted in Fig. 8 for simulations with $r_d = 2/3000$ (a) and $1/30$ (b) for one run (solid line) and compared with the monodisperse case (dashed line) and the average over 100 runs (symbols). The fluctuations of the stresses increase with growing r_d. In fact we observe fluctuations much larger than the total stress for the monodisperse pile. With increasing r_d the shape of the averaged vertical stress changes in the center from a hump [see $r_d = 2/3000$] to a dip [see $r_d = 1/30$]. The averaged stress in Fig. 8(b) is similar to the stress obtained (after many averages) from a cellular automaton model for the stress propagation in the presence of randomly opened contacts [90].

In Fig. 9 the contact network of one representative run from Fig. 8(b) is displayed. The lines correspond to the branch vectors $\vec{l}$ and their thickness indicates the magnitude of forces active at the corresponding contact. Each particle center is thus located at the meeting point of several lines. When counting the number of contacts from one run for all layers $M \geq 1$, we obtain a coordination number of 3.9616; when disregarding also the particles at the surface, one comes closer to the value of 4 that could be expected for an isostatic situation. We attribute the discrepancy to those particles with few contacts, e.g. on the surface and inside the material but screened by an arch. Also, the heap could be not completely relaxed, so that a few (weak) contacts are either missing, or active whereas they would be active or missing, respectively, when relaxation would be total.

Already tiny polydispersity destroys the regular, periodic contact network. Due to the small fluctuations in particle size the particles are still positioned on a triangular lattice even when the contacts are randomly open. In such a random network the so called stress chains, i.e. selected paths of large stresses, are found and the stress fluctuations can become much larger than the average stress. Averaging over disordered systems and many realizations leads to a dip in the vertical stress at the bottom if the size fluctuations are sufficiently

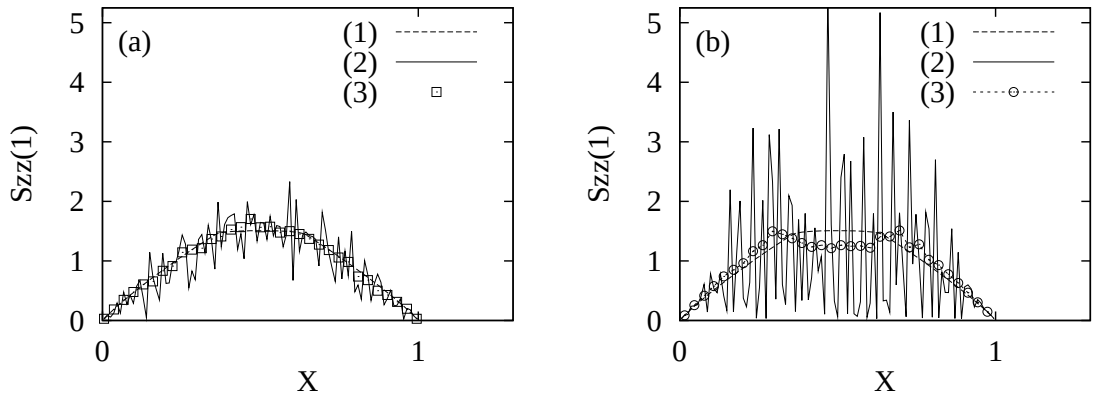

Figure 8: Dimensionless vertical stress $S_{zz}(1)$, in row $M = 1$, vs. X for a 30^o pile with bumpy bottom and $L_1 = 97$, from [23]. The particle diameter is uniformly distributed in the interval $[d_0(1 - r_d/2), d_0(1 + r_d/2)]$, with $r_d = 2/3000$ (a) and $r_d = 1/30$ (b). The dashed line gives the result with no disorder $r_d = 0$ and $L_1 = 97$. The solid line gives the result of one representative run and the symbols correspond to an average over 100 runs and three particles.

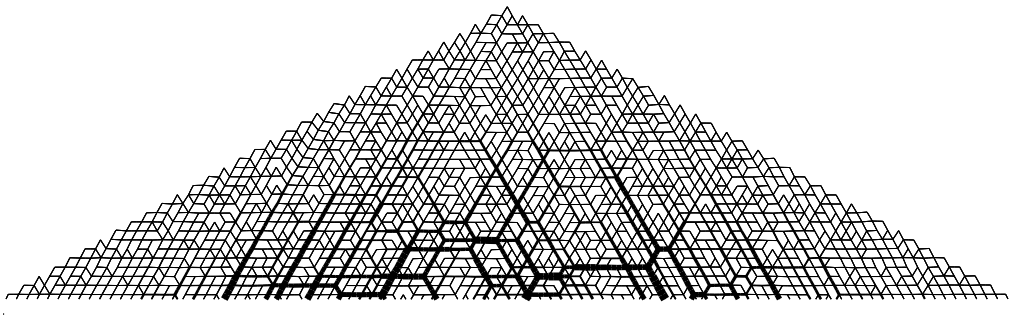

Figure 9: Contact network of one pile from Fig. 8(b). The line thickness indicates the magnitude of the contact force, from [23].

large [23]. Note that the transition from a homogeneous network to the stress chains is controlled by the ratio of the size fluctuations $r_d\, d$ and the particle overlap δ, but not by the size fluctuations alone. Since the particle overlap is a function of the particle stiffness and of the local stress, $\delta \propto \sigma d^2/k_n$, the dimensionless parameter that measures the strength and the effect of the fluctuations is $\varrho = r_d k_n/(\sigma d)$. If $\varrho \ll 1$ the fluctuations in particle size are negligible, if $\varrho \gg 1$ one can expect essential disorder in the system, even if $r_d \ll 1$.

Measuring the probability distribution of the forces, one observes results in agreement with theoretical predictions [15], and numerical findings [16]. The probability to find large stresses decreases exponentially with the magnitude of the stress and is greater for smaller r_d, i.e. for stronger fluctuations [23]. The important result is, however, that disorder in the system changes the qualitative outcome, i.e. a dip is found in the polydisperse case, even when no dip is present in the ordered situation. Since we were able to find most of the phenomenology expected in a sandpile in an oversimplified regular model system without friction, we conclude that the role of the contact network (or the fabric) is eminent. Nevertheless, friction and polydispersity in size and shape will play a role in more general situations with physical sandpiles made of realistic, non-spherical particles.

5 Results with polygonal particles

In the previous section, the particles were spherical, and almost mono-disperse, resembling a "cannon-ball" piling, a stack of smooth, wooden rods, or a model granulate like glass beads. Since granular materials can be by far more complicated, concerning their size distribution and their shape as well, convex polygons are used in the following as a model for, e.g. sand-grains or crushed glass.

5.1 A brief review of some experiments

From experiments on large piles, Brockbank et al. [29] found no dip, i.e. no pressure minimum under the apex of the pile, for large (non-cohesive) monodisperse particles poured on a flat surface from a point-source. With the same construction mode, but using polydisperse material Smid and Novosad [28] found a pronounced dip under the apex of the pile. The only data from cones for which the minimum pressure was less than 15 % smaller than the maximum pressure was obtained for monodisperse rape seed [28].

Jotaki et al. [26] examined a variety of materials with different properties, sizes and shapes as summarized in table 1. One of the most striking results of these experiments is that for polydisperse materials the pressure under the apex of the pile (also created from a point-source) is about 20% to 30% smaller than the maximum pressure. This occurs in granular materials with very different internal friction and angles of repose, see table 1. It

Material	Pressure Dip [%]	Angle of repose [deg]	Particle size [mm]	Coeff. of int. friction
GB 708	81	22.5	0.3-0.7	0.41
GB 733	60	22.7	0.044-0.088	0.27
Sea Sand	77	33.6	0.17-0.71	0.60
Rape Seed	87	24.9	1.4	0.40

Table 1: Parameters for the grains in the heaps used by Jotaki et al. [26]

should be noted that the angles of repose range from 22.5^o to 33.6^o, whereas the coefficients of internal friction span a wider range from 0.27 to 0.61. The angle of repose and the internal friction are not necessarily proportional, as can be seen from table 1, but there appears to be a correlation between large angles of internal friction and a wide variation in particle size.

Concerning the grain size 1.4 mm, given for rape seed, and the base diameter of the largest heaps being 120 mm to 320 mm, there were about 100 to 140 particles in the base of the smaller systems [26]. Smid and Novosad [28] examined piles of fertilizer with base lengths from 600 mm up to 1700 mm. Fertilizer has a grain size of 3 to 5 mm, which also leads to a system size of 100 to several hundreds of particles. The simulations presented in the following use 100 to 140 particles in the horizontal direction, so that the base length is comparable to the one in the experimental heaps, measured in units of the particle diameter.

5.2 Polygonal particles on an ordered grid

First, monodisperse regular polygons with $C = 12$ sides (or corners), initially ordered on a hexagonal lattice, are used. The results, with $\mu = 0$, were already displayed in Fig. 6 and are denoted by (h1). The data for larger coefficients of friction $\mu = 0.3$ and $\mu = 0.6$ are denoted by (h2) and (h3) respectively. The angle of repose of the heaps is by construction 30^o. The base of the heap is $L_0 = 100$ particle diameters in the lowermost layer, where the particles are fixed. The heaps are built layer by layer and then relaxed until most of the energy is

dissipated. The stress distribution for the heap on the hexagonal lattice for $\mu = 0.0$, 0.3, 0.6 did not change noticeably with the friction coefficient μ, see Fig. 10. The fluctuations for the situations with friction (h2, h3) are much stronger than in the frictionless case (h1). However, the stresses are similar in magnitude and shape.

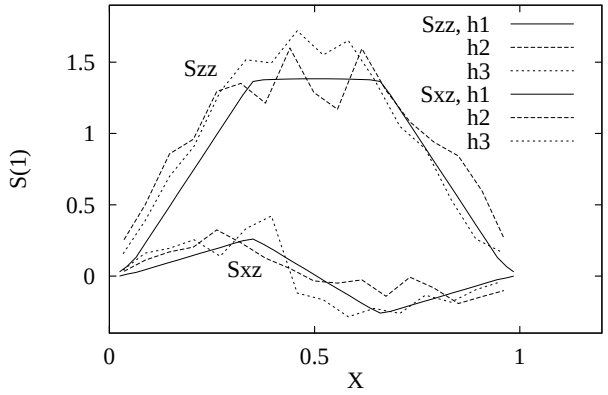

Figure 10: Stress distribution S_{zz} and S_{xz} for the different heaps with the coefficients of friction $\mu = 0$ (h1), $\mu = 0.3$ (h2) and $\mu = 0.6$ (h3).

No clear relative minimum of the normal stress in the center of the heaps can be observed for the parameters and configurations presented here. Mounting the lowermost layer on springs (no figures shown) and permitting vertical motion did not change the qualitative outcome of the simulations, for some more information on this issue see chapter 1 in [13]. Since the monodisperse polygons with many corners are very close to spheres, polygons with less corners and also of more elongated shape will be used in the following and also the construction

5.3 A typical microscopic configuration

For comparison with Fig. 9, we present a contact network of one simulation with flat frictional bottom and $N = 3333$ particles of different shapes, which were obtained by inscribing polygons with $C = 7$ corners into ellipses with uniformly distributed axes $a = 9.5 \pm 1.5\,\mathrm{mm}$ and $b = 9.5 \pm 1.5\,\mathrm{mm}$. The particles were simulated as rods of 1 m length with a material density of $\rho_{\mathrm{mat}} = 5000\,\mathrm{kg/m^3}$, and a stiffness $k^{\mathrm{n}} = 10^7\,\mathrm{N/m}$. The coefficient of friction was $\mu = 0.6$, and the dimensionless damping constant in Eq. (7) was $\eta^{\mathrm{n}} = 0.8$. The timestep for the simulation was $\Delta t = 2.5 \times 10^{-5}\,\mathrm{s}$ and a fifth order Gear predictor-corrector method was used. A new particle was added from a point-source to the system every 0.075 s, up to time $t = 250\,\mathrm{s}$. The snapshot corresponds to the relaxed situation taken at $t = 260\,\mathrm{s}$.

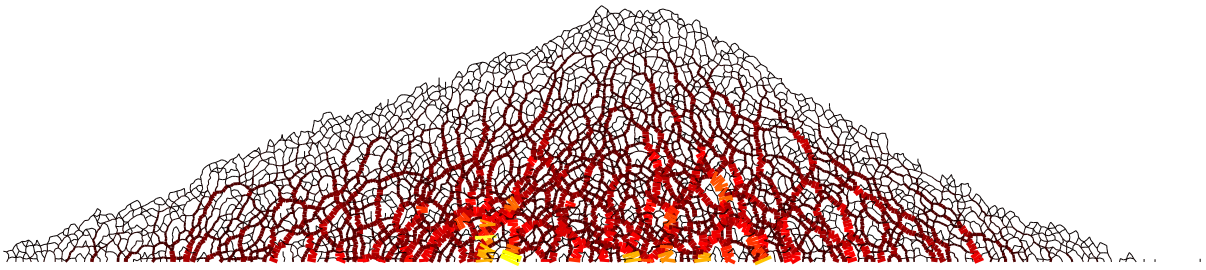

Figure 11: Force network of a heap constructed from a point source on a flat bottom.

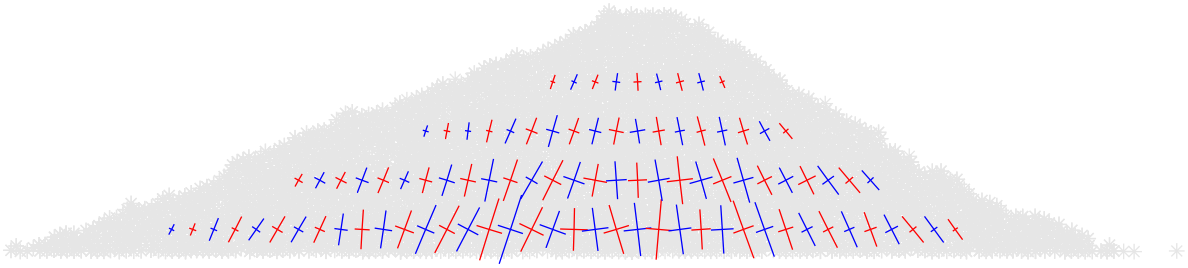

Figure 12: Stresses in the principal axis representation, inside the heap from Fig. 11, averaged over volumes containing 40-50 particles.

The force-network of the simulation is displayed in Fig. 11. Both the outline and the structure of the network are different from the ordered situation displayed in Fig. 9. The outline and the stress chains indicate the disorder of the heap, and also the principal axes of the stress tensor are strongly fluctuating, see Fig. 12. The principal axes of the stress tensor are obtained by moving averages in horizontal direction, where an averaging volume covers 40 to 50 particles. The pressure dip can be seen in the principal stresses plot. In the outer part of the pile, the orientation of the stress tensor is almost constant (especially in the right half), in agreement with the FPA assumption by Wittmer et al. [86].

5.4 The construction history

To model experiments as realistically as possible, one can construct a pile in two ways, both of technical relevance: Pouring the sand from an outlet, say a point-source, is the variant which will be used in chemical engineering, e.g. in the filling of silos, or when building a heap of material that is transported on a conveyor belt. On the other hand, in civil engineering, dams are constructed layerwise. This leads to a different "history" of the particles in the heap, which can be seen by the different strata of the heaps in Fig. 13. Particles of different grey are poured on the pile at different times. In these simulations, irregular heptagons with $C = 7$ corners are used, which were inscribed to an ellipse with different axes. The irregularity was introduced by changing the starting point on the ellipse, whereas the length of the two axis of the ellipses were changed to get polydisperse particles (rods of length 1 m). The material density was $\rho_{\mathrm{mat}} = 5000\,\mathrm{kg/m^3}$, the contact stiffness was $k^{\mathrm{n}} = 10^7\,\mathrm{N/m}$, and the dimensionless damping coefficient was $\eta^{\mathrm{n}} = 0.5$. The friction coefficient was set to $\mu = 0.6$ for the particle-particle and for the particle-wall interaction as well in order to resemble the friction of sea sand, see table 1. The time-steps are varied between $\Delta t = 10^{-5}\,\mathrm{s}$ and $\Delta t = 2.5 \cdot 10^{-5}\,\mathrm{s}$ depending on the minimum particle radius.

5.4.1 The wedge sequence

Here we examine the stress under piles on a flat bottom, built from a point source – this procedure is named wedge sequence in the following – and compare material of different polydispersity. The particles were dropped from 40 cm height with 0.2 m/s initial velocity. Due to the large impact velocity, the top of the pile at height h is usually flat, the angle of repose, see table 2, was measured in that part of the pile where the slope is straight. In order to suppress the fluctuations, we used "moving averages" as described in section 3. In Fig. 14(a), data are shown for different polydispersities. Additional runs with different random number seeds gave equivalent results within the fluctuations. The pressure dip is qualitatively

Sequence	Slope [deg]	Particle size $a \times b$ [mm]	Particles	h [m]	l [m]	M [10^3 kg]
Wedge	23	4 × 5	2600	0.13	0.61	1.5
Wedge	24	4 × 4-5.5	4000	0.17	0.88	3.2
Wedge	28	2-5.5 × 2-5.5	2000	0.11	0.46	1.2
Layered	32	4 × 4-5.5	3400	0.18	0.69	2.7

Table 2: Parameters for the presented simulations of heaps built either in the layered or in the wedge sequence. The data points were obtained by a moving average procedure with a bin-width of about 14 particle diameters. The layered sequence is explained in the following subsection.

comparable to the pressure dip obtained from experiments only for the simulations with polydisperse particles: there is no evidence of a dip in the case of monodisperse particles.

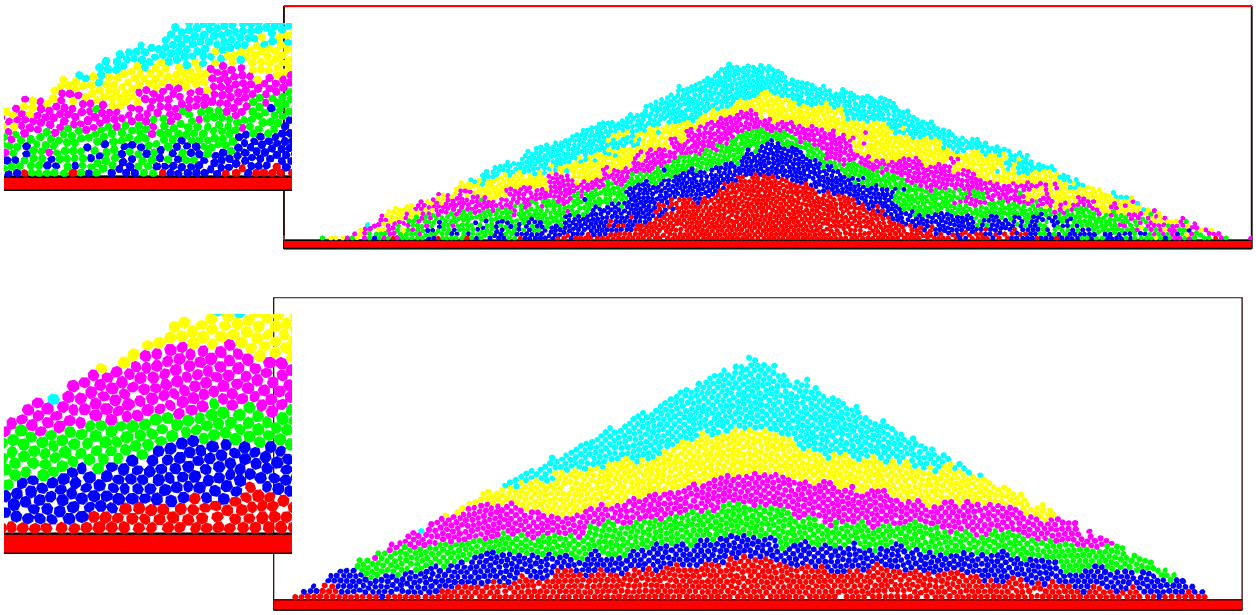

Figure 13: Configuration for a wedge sequence with polydisperse particles, where the pile is constructed from a point source (top), and a layered sequence with monodisperse particles (bottom). Different shading indicates the different age of the particles. The insets are zooms into the lower left part of the corresponding pile.

5.4.2 The layered sequence

When the pile is constructed in a layered sequence, it is build by dropping particles smoothly from a height of less than one particle diameter onto the already present layers. Each new layer is less wide than the previous one to arrive at the desired outline of the pile. Settling effects in the strata of the system are visible in Fig. 13, and the pressure data are shown in Fig. 14(b), indicating no dip. Another important result is that the angle of repose of a pile constructed in the layered sequence, see table 2, is larger than for the wedge sequence with the same size distribution. One reason for the smaller angle of repose of the piles build in wedge sequence can be the rather large impact velocity of the particles. Another effect, that is also likely to affect strongly the internal structure of the pile and its slope, is avalanching at the surface which occurs several times when a pile is constructed in the wedge sequence.

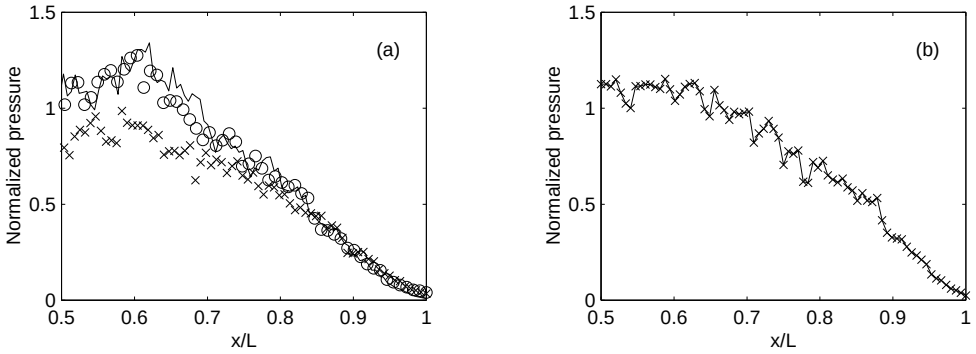

Figure 14: (a) Scaled vertical stress $S^* = 2\sigma/(\rho_{\mathrm{mat}} g h)$ under two dimensional heaps built from a point source (wedge sequence). The data do not scale, since the packing density (is smaller than the material density) and different from one simulation to the other. The lowermost data (crosses) correspond to the monodisperse case, while the solid line and the circles correspond to medium and strong polydispersity, respectively, see table 2 for details. (b) Scaled vertical stress at the bottom of a two dimensional heap built in the layered sequence with medium polydispersity, see table 2.

Our data indicate that the presence of the dip depends on the construction history of the pile. Seemingly, the construction from a point-source leads to avalanches and reorganizations that enhance arching whereas a careful build-up layer by layer hinders arching and leads to a more homogeneous stress inside the pile. Since the ground was flat and non-deformable, for all simulations presented here, the different magnitude of the dip shows that the bending of the bottom due to the elasticity of its material cannot be the only reason for the dip. For understanding, why this is important and controversal, see the paper by Savage in [13]. The dip is more likely to occur for more polydisperse material and for the construction from a point source.

6 Summary and Discussion

From the systems with smooth, spherical particles, several interesting facts could be extracted. First, the structure of the contact network and its orientation is correlated to the stress state. Isotropic stress corresponds to an isotropic, triangular contact network, whereas anisotropic stress is connected to a diamond network with inhomogeneous stiffness of the material. Second, already small variations of either boundary conditions or particle sizes leads to arching and sometimes a dip can be found. Third, these results do not depend much on details of the interaction law or on the particle shape as long as the surfaces are smooth. Therefore we modeled in addition polygons with friction. When the polygons are almost spherical, with $C = 12$ corners, the stress in the pile is similar to the case of a pile of spherical particles. Only, when the particles are set up with more size and shape polydispersity more interesting results are obtained. The piles can be constructed either layerwise or from a point source in a so-called wedge sequence. The layered sequence resembles a slow and careful construction, whereas the wedge sequence is usually applied to deposit granulates from a conveyor belt. Measuring the angle of repose and the forces at the bottom of the piles, one observes: (i) The angle of repose depends on the construction history. If the pile is constructed slowly and layerwise, it has a larger angle of repose than a pile constructed in a wedge sequence. (ii) The angle of repose also depends on the polydispersity of the material.

The more spherical the particles are, the smaller is the measured angle of repose, given that the construction histories are identical. (iii) We find evidence of a dip in the vertical stress under the apex of the heap when the pile is constructed in a wedge sequence, but only if (iv) the particles are eccentric. (v) For the same polydispersity, but for a layerwise construction, no dip is observed.

In simplified model systems with smooth, spherical particles most of the phenomenology (as stress chains and arching) is found, but our impression is that a nonspherical particle shape contributes in addition and is of eminent importance for the quantitative comparison of numerical simulations with experimental data. However, it is still interesting to examine also the model-systems with spherical particles, since their simple geometry allows treatable theoretical approaches to predict the fabric- and stress-distribution in dense packings. Whereas the two dimensional polygonal particles are used in simulations many years, the simulation of polygonal particles in three dimensions is still a rarely addressed issue as well as the modeling of rolling friction and the friction due to rotation about the contact normal, effects which will play a role in realistic situations.

Acknowledgements

We thank our colleagues Gadi Oron, and Alexander Schinner for their courtesy to allow us to present parts of their work in this paper. Furthermore, we acknowledge the support of the Deutsche Forschungsgemeinschaft, Sonderforschungsbereich 382 (project A6).

References

[1] M. H. Cooke, D. J. Stephens, and J. Bridgewater. Powder mixing - a literature survey. *Powder Technol.*, 15:1, 1976.

[2] C. S. Campbell. Rapid granular flows. *Annu. Rev. Fluid Mech.*, 22:57, 1990.

[3] D. Geldart and M. J. Rhodes. Survey of current world-wide research in gas fluidization (jan. 1989 - dec. 1991). *Powder Technol.*, 71:1, 1992.

[4] H. M. Jaeger and S. R. Nagel. Physics of the granular state. *Science*, 255:1523, 1992.

[5] H. M. Jaeger, S. R. Nagel, and R. P. Behringer. The physics of granular materials. *Physics Today*, 49(4):32–38, 1996.

[6] H. M. Jaeger, S. R. Nagel, and R. P. Behringer. Granular solids, liquids, and gases. *Reviews of Modern Physics*, 68(4):1259–1273, 1996.

[7] H. J. Herrmann and S. Luding. Modeling granular media with the computer. *Continuum Mechanics and Thermodynamics*, 10:189–231, 1998.

[8] A. Hansen and D. Bideau, editors. *Disorder and Granular Media.* North Holland, Amsterdam, 1992.

[9] C. Thornton, editor. *Powders & Grains 93.* Balkema, Rotterdam, 1993.

[10] A. Mehta, editor. *Granular Matter.* Springer, Berlin, 1994.

[11] D. E. Wolf and P. Grassberger, editors. *Friction, Arching and Contact Dynamics.* World Scientific, Singapore, 1997.

[12] R. P. Behringer and J. T. Jenkins, editors. *Powders & Grains 97*. Balkema, Rotterdam, 1997.

[13] H. J. Herrmann, J.-P. Hovi, and S. Luding, editors. *Physics of dry granular media - NATO ASI Series E 350*. Kluwer Academic Publishers, Dordrecht, 1998.

[14] H. A. Janssen. Versuche über Getreidedruck in Silozellen. *Zeitschr. d. Vereines deutscher Ingenieure*, 39(35):1045–1049, 1895.

[15] C.-h. Liu, S. R. Nagel, D. A. Schecter, S. N. Coppersmith, S. Majumdar, O. Narayan, and T. A. Witten. Force fluctuations in bead packs. *Science*, 269:513, 1995.

[16] F. Radjai, M. Jean, J. J. Moreau, and S. Roux. Force distribution in dense two-dimensional granular systems. *Phys. Rev. Lett.*, 77(2):274, 1996.

[17] S. N. Coppersmith, C.-h. Liu, S. Majumdar, O. Narayan, and T. A. Witten. Model for force fluctuations in bead packs. *Phys. Rev. E*, 53(5):4673–4685, 1996.

[18] S. Ouaguenouni and J.-N. Roux. Arching without friction: a simple model. In D. E. Wolf and P. Grassberger, editors, *Friction, Arching and Contact Dynamics*, Singapore, 1997. World Scientific.

[19] D. C. Hong. Stress distribution of a hexagonally packed granular pile. *Phys. Rev. E*, 47(1):760–762, 1993.

[20] K. Liffman, D. Y. C. Chan, and B. D. Hughes. On the stress depression under a sandpile. *Powder Technol.*, 78:263–271, 1994.

[21] J.-P. Bouchaud, M. E. Cates, and P. Claudin. Stress distribution in granular media and nonlinear wave equation. *J. Phys. I*, 5:639–656, 1995.

[22] J. P. Wittmer, M. E. Cates, and P. Claudin. Stress propagation and arching in static sandpiles. *J. Phys. I*, 7:39–80, 1997.

[23] S. Luding. Stress distribution in static two dimensional granular model media in the absence of friction. *Phys. Rev. E*, 55(4):4720–4729, 1997.

[24] H.-G. Matuttis. Simulations of the pressure distribution under a two dimensional heap of polygonal particles. *Granular Matter*, 1(2):83–91, 1998.

[25] F. H. Hummel and E. J. Finnan. The distribution of pressure on surfaces supporting a mass of granular material. *Proc. Instn. Civil Engn.*, 212:369–392, 1921. the former: Minutes of Proc. of the Instn. of civil Engineers with other selected papers.

[26] T. Jotaki and R. Moriyama. On the bottom pressure distribution of the bulk materials piled with the angle of repose. *Journal of the Society of Powder Technology, Japan*, 16(4):184–191, 1979.

[27] D. H. Trollope and B. C. Burman. Physical and numerical experiments with granular wedges. *Géotechnique*, 30(2):137–157, 1980.

[28] J. Šmid and J. Novosad. Pressure distribution under heaped bulk solids. *I. Chem. E. Symposium Series*, 63:D3/V/1–12, 1981.

[29] R. Brockbank, J. M. Huntley, and R.C. Ball. Contact force distribution beneath a three-dimensional granular pile. *J. Phys. II France*, 7:1521–1532, 1997.

[30] I. K. Lee and J. R. Herrington. Stresses beneath granular embarkments. *Proceedings of the first Australian-New Zealand Conference on Geomechanics: Melbourne*, 1:291–296, August 1971.

[31] B. Lackinger. *Das Tragverhalten von Staudämmen mit membranartigen Dichtungen.* PhD thesis, Mitteilungen des Instituts für Bodenmechanik, Felsmechanik und Grundbau an der Fakultät für Bauingenieurwesen und Architekture der Universität Innsbruck, 1980.

[32] P. A. Cundall and O. D. L. Strack. A discrete numerical model for granular assemblies. *Géotechnique*, 29(1):47–65, 1979.

[33] R. J. Bathurst and L. Rothenburg. Micromechanical aspects of isotropic granular assemblies with linear contact interactions. *J. Appl. Mech.*, 55:17, 1988.

[34] C. Thornton. Force transmission in granular media. *KONA Powder and Particle*, 15:81–90, 1997.

[35] C. Thornton and C. W. Randall. Applications of theoretical contact mechanics to solid particle system simulation. In *Micromechanics of granular media*, Amsterdam, 1988. Elsevier.

[36] Y. M. Bashir and J. D. Goddard. A novel simulation method for the quasi-static mechanics of granular assemblages. *J. Rheol.*, 35(5):849–885, 1991.

[37] R. Dobry and T. T. Ng. Discrete modelling of stress-strain behaviour of granular media at small and large strains. *Eng. Comput.*, 9:129–143, 1992.

[38] C. Thornton and S. J. Antony. Quasi-static deformation of particulate media. submitted to: Phil. Trans. Roy. Soc. A, 1998.

[39] C. Thornton. Numerical simulations of deviatoric shear deformation of granular media. submitted to: Géotechnique, 1998.

[40] John M. Ting. A robust algorithm for ellipse-based discrete element modelling of granular materials. *Computers and Geotechnics*, 13:175–186, 1992.

[41] L. Meachum J. M. Ting, J. D. Rowell. Influence of particle shape on the strengh of ellipse-shaped granular assemblages. In John R. Williams, editor, *Proceedings on the 2nd International Conference on Discrete Element Methods (DEM)*, pages 215–225, Cambridge, Mass, 1993. IESL Publ.

[42] T. T. Ng. Numerical simulations of granular soil using elliptical particles. In *Microstructural characterization in Constitutive Modeling of Metals and Granular Media: presented at the ASME Summer Mechanics and Materials Conferences*, volume MD-Vol. 32. ASME, April 28-May 1 1992.

[43] J. R. Williams and A. P. Pentland. Superquadrics and modal dynamics for discrete elements in interactive design. *Eng. Comput.*, 9:115–127, 1992.

[44] A. V. Potapov and C. S. Campbell. A fast model for the simulation of non-round particles. *Granular Matter*, 1(1):9–14, 1998.

[45] R. Barbosa and J. Ghaboussi. Discrete finite element method. *Eng. Comput.*, 9:253–266, 1992.

[46] J. A. Issa and R. B. Nelson. Numerical analysis of micromechanical behaviour of granular materials. *Eng. Comput.*, 9:211–223, 1992.

[47] G. Hocking. The discrete element method for analysis of fragmentation of discontinua. *Eng. Comput.*, 9:145–155, 1992.

[48] H.-J. Tillemans and H. J. Herrmann. Simulating deformations of granular solids under shear. *Physica A*, 217:261–288, 1995.

[49] F. Kun and H. J. Herrmann. Fragmentation of colliding discs. *Int. J. of Mod. Phys. C*, 7(6):837–855, 1996.

[50] N. P. Kruyt and L. Rothenburg. Micromechanical definition of strain tensor for granular materials. *ASME Journal of Applied Mechanics*, 118:706–711, 1996.

[51] C.-L. Liao, T.-P. Chang, D.-H. Young, and C. S. Chang. Stress-strain relationship for granular materials based on the hypothesis of best fit. *Int. J. Solids Structures*, 34:4087–4100, 1997.

[52] M. P. Allen and D. J. Tildesley. *Computer Simulation of Liquids.* Oxford University Press, Oxford, 1987.

[53] D. C. Rapaport. *The Art of Molecular Dynamics Simulation.* Cambridge University Press, Cambridge, 1995.

[54] O. R. Walton. Force models for particle-dynamics simulations of granular materials. In E. Guazzelli and L. Oger, editors, *Mobile Particulate Systems*, page 367, Dordrecht, 1995. Kluwer Academic Publishers.

[55] J. Schäfer, S. Dippel, and D. E. Wolf. Force schemes in simulations of granular materials. *J. Phys. I France*, 6:5–20, 1996.

[56] S. Luding. Collisions & contacts between two particles. In H. J. Herrmann, J.-P. Hovi, and S. Luding, editors, *Physics of dry granular media - NATO ASI Series E350*, page 285, Dordrecht, 1998. Kluwer Academic Publishers.

[57] O. R. Walton. Numerical simulation of inelastic, frictional particle-particle interactions. In M. C. Roco, editor, *Particulate two-phase flow*, page 884, Boston, 1993. Butterworth-Heinemann.

[58] G. Lian, M. J. Adams, and C. Thornton. Elastohydrodynamic collisions of solid spheres. *J. Fluid Mech.*, 311:141, 1996.

[59] S. F. Foerster, M. Y. Louge, H. Chang, and K. Allia. Measurements of the collision properties of small spheres. *Phys. Fluids*, 6(3):1108–1115, 1994.

[60] L. Labous, A. D. Rosato, and R. Dave. Measurements of collision properties of spheres using high-speed video analysis. *Phys. Rev. E*, 56:5715, 1997.

[61] E. Falcon, C. Laroche, S. Fauve, and C. Coste. Behavior of one inelastic ball bouncing repeatedly off the ground. *Eur. Phys. J. B*, 3:45–57, 1998.

[62] H. Hertz. Über die Berührung fester elastischer Körper. *J. für die reine u. angew. Math.*, 92:136, 1882.

[63] L. D. Landau and E. M. Lifshitz. *Elasticity Theory.* Pergamon Press, Oxford, 1975.

[64] O. R. Walton and R. L. Braun. Viscosity, granular-temperature, and stress calculations for shearing assemblies of inelastic, frictional disks. *Journal of Rheology*, 30(5):949–980, 1986.

[65] C. Thornton. Coefficient of restitution for collinear collisions of elastic-perfectly plastic spheres. *Journal of Applied Mechanics*, 64:383–386, 1997.

[66] G. Kuwabara and K. Kono. Restitution coefficient in a collision between two spheres. *Japanese Journal of Applied Physics*, 26(8):1230–1233, 1987.

[67] S. Luding, E. Clément, A. Blumen, J. Rajchenbach, and J. Duran. Anomalous energy dissipation in molecular dynamics simulations of grains: The "detachment effect". *Phys. Rev. E*, 50:4113, 1994.

[68] N. V. Brilliantov, F. Spahn, J. M. Hertzsch, and T. Pöschel. Model for collisions in granular gases. *Phys. Rev. E*, 53(5):5382, 1996.

[69] J. Lee and H. J. Herrmann. Angle of repose and angle of marginal stability: Molecular dynamics of granular particles. *J. Phys. A*, 26:373, 1993.

[70] L. Brendel and S. Dippel. Lasting contacts in molecular dynamics simulations. In H. J. Herrmann, J.-P. Hovi, and S. Luding, editors, *Physics of Dry Granular Media*, page 313, Dordrecht, 1998. Kluwer Academic Publishers.

[71] F. Radjai, J. Schäfer, S. Dippel, and D. Wolf. Collective friction of an array of particles: A crucial test for numerical algorithms. *J. Phys. I France*, 7:1053, 1997.

[72] O. R. Walton and R. L. Braun. Simulation of rotary-drum and repose tests for frictional spheres and rigid sphere clusters. In *DOE/NSF Workshop on Flow of Particulates and Fluids*, pages 1–17, 1993.

[73] V. Buchholtz, T. Pöschel, and H.-J. Tillemans. Simulation of rotating drum experiments using non-circular particles. *Physica A*, 216:199, 1995.

[74] V. Buchholtz and T. Pöschel. Numerical investigations of the evolution of sandpiles. *Physica A*, 202:390, 1994.

[75] G. A. Kohring, S. Melin, H. Puhl, H. J. Tillemans, and W. Vermöhlen. Computer simulations of critical, non-stationary granular flow through a hopper. *Comput. Methods in Appl. Mechanics and Eng.*, 124:2273, 1995.

[76] H.-G. Matuttis and S. Luding. The effect of particle shape and friction on the stresses in heaps of granular media. In D. E. Wolf and P. Grassberger, editors, *Friction, Arching and Contact Dynamics*, Singapore, 1997. World Scientific.

[77] G.-H. Shi. Discontinous deformation analysis: A new numerical model for the statics and dynamics of deformable block structures. *Eng. Comput.*, 9:157–168, 1992.

[78] J. Krishnasamy and M. J. Jakiela. A method to resolve ambiguities in corner-corner interactions between polygons in the context of motion simulations. *Eng. Comput.*, 12:135–144, 1995.

[79] T. Pöschel and V. Buchholtz. Molecular dynamics of arbitrarily shaped granular particles. *J. Phys. I France*, 5(11):1431–1455, 1995.

[80] A. Munjiza, D. R. J. Owen, and N. Bicanic. A combined finite-discrete element method in transient dynamics of fracturing solids. *Eng. Comput.*, 12:145–174, 1995.

[81] H.-J. Tillemanns. *Molekulardynamik beliebig geformter Teilchen in zwei Dimensionen.* PhD thesis, Universität Köln, 1995.

[82] J. D. Goddard. Microstructural origins of continuum stress fields - a brief history and some unresolved issues. In D. DeKee and P. N. Kaloni, editors, *Recent Developments in Structered Continua. Pitman Research Notes in Mathematics No. 143*, page 179, New York, 1986. Longman, J. Wiley.

[83] K. Liffman, D. Y. C. Chan, and B. D. Hughes. Force distribution in a two dimensional sandpile. *Powder Technol.*, 72:255–267, 1992.

[84] S. van Baars. *Discrete Element Analysis of Granular Materials.* PhD thesis, Technische Universiteit Delft, Delft, Nederlands, 1996.

[85] G. Oron and H. J. Herrmann. Exact calculation of force networks in granular media. *Phys. Rev. E*, 58(2):2079–2089, 1998. cond-mat/9707243.

[86] J. P. Wittmer, P. Claudin, M. E. Cates, and J.-P. Bouchaud. An explanation for the central stress minimum in sand piles. *Nature*, 382:336–338, 1996.

[87] S. Luding and H.-G. Matuttis. The effect of interaction laws on the stresses in frictionless granular media. In D. E. Wolf and P. Grassberger, editors, *Friction, Arching and Contact Dynamics*, pages 207–211, Singapore, 1997. World Scientific.

[88] S. F. Edwards and C. C. Mounfield. A theoretical model for the stress distribution in granular matter. III: Forces in sandpiles. *Physica A*, 226:25, 1996.

[89] G. Oron and H. J. Herrmann. Exact determination of force networks in a static assembly of disks. In H. J. Herrmann, J.-P. Hovi, and S. Luding, editors, *Physics of Dry Granular Media*, page 143, Dordrecht, 1998. Kluwer Academic Publishers.

[90] J. Hemmingsson, H. J. Herrmann, and S. Roux. On stress networks in granular media. *J. Phys. I*, 7:291–302, 1997.